THE ASTROPHYSICAL JOURNAL, 295:258–274, 1985 August 1

EVIDENCE FOR COLLISIONLESS CONDUCTION FRONTS IN IMPULSIVE SOLAR FLARES

DAVID A. BATCHELOR[1] AND CAROL JO CRANNELL
Laboratory for Astronomy and Solar Physics, NASA/Goddard Space Flight Center, Greenbelt, Maryland
AND
HERBERT J. WIEHL AND ANDREAS MAGUN
Institute of Applied Physics, University of Bern, Bern, Switzerland
Received 1984 July 10; accepted 1985 February 5

ABSTRACT

Impulsive bursts of hard X-rays and microwaves are observed during most solar flares, and both emissions can be attributed to a common distribution of source electrons with energies from approximately 10 keV to several hundred keV. A detailed account of the evolution of the electron distribution is crucial to a complete description of the energy release process in flares. In this paper, a new analysis is made of a thermal flare model proposed by Brown, Melrose, and Spicer; and Smith and Lilliequist. They argued that the source assumed in this model would not explain the simultaneous impulsive microwave emission. In contrast, the new results presented here show that this model leads to the development of a quasi-Maxwellian distribution of electrons that explains both the hard X-ray and microwave emissions. This implies that the source sizes can be determined from observations of the optically thick portions of microwave spectra and the temperatures obtained from associated hard X-ray observations. In this model, the burst emission would rise to a maximum in a time t_r approximately equal to L/c_s, where L is the half-length of the arch, and $c_s = (kT_e/m_i)^{1/2}$ is the ion-sound speed. New observations of these impulsive flare emissions are analyzed herein to test this prediction of the model. The X-ray observations were obtained with the Hard X-Ray Burst Spectrometer on board the *Solar Maximum Mission* spacecraft, and the microwave observations were obtained from the Bern Radio Observatory in Switzerland. Electron densities of order 10^9 cm^{-3}, source sizes of order 10^{18} cm^2, magnetic field strengths of order 10^2 G, and total burst energies of order 10^{28} ergs are derived from the observations. The results of this investigation are in good agreement with the model and are not explained by any other flare models which have been considered.

Subject headings: plasmas — radiation mechanisms — Sun: flares — Sun: radio radiation — Sun: X-rays

I. INTRODUCTION

Energetic electrons in solar flares manifest their presence through a variety of emission mechanisms, and play an important role in the energy transport and total energy budget of a given flare (see reviews by Brown 1975, 1976; Brown and Smith 1980). In particular, electrons with energies $\gtrsim 30$ keV produce hard X-rays by collisional bremsstrahlung with atomic nuclei and microwaves by the gyroscynchrotron process. Time histories of these two emissions are often very similar and both emissions can, in principle, be attributed to a common distribution of source electrons.

One of the most crucial and controversial questions about solar flares is whether the impulsive hard X-rays and microwave bursts originate in a thermal or nonthermal population of energetic electrons. In nonthermal models, the hard X-rays are produced by accelerated electrons as they interact with the constituents of the ambient medium. This process is very inefficient because only one part in 10^5 of the total energy loss goes into the production of hard X-rays. The most efficient of the nonthermal models, the thick-target model, invokes intense electron beams created in the corona and incident upon the chromosphere. Doubts about the prospects for creation and stabilization of such beams have been raised by Smith (1975), Melrose and Brown (1976), Hoyng, Brown, and van Beek (1976), Hoyng, Knight, and Spicer (1978), and Colgate (1978). In addition, Brown *et al.* (1983) have shown that the temporal evolution of the height structures of five impulsive flares is entirely inconsistent with the thick-target model of hard X-ray bursts. Renewed interest in thermal-flare models has been kindled by these difficulties with nonthermal models and by recognition of the potentially greater emission efficiency of a confined, collisionally relaxed X-ray source. Detailed discussions of these points are given by Crannell *et al.* (1978), Mätzler *et al.* (1978), Brown, Melrose, and Spicer (1979, hereafter BMS), and Smith and Lilliequist (1979, hereafter SL). No observational evidence has been published to date, however, that distinguishes unambiguously between the two classes of models.

In this paper, new observations of impulsive hard X-ray and microwave bursts are analyzed, and the results are compared with predictions of a particular thermal flare model which has received much attention in the literature. In the model, both emissions are assumed to originate in a hot plasma at a temperature of order 10^8 K (Chubb 1972; Crannell *et al.* 1978). The plasma is effectively confined by the development of collisionless conduction fronts, as proposed by BMS and by SL. In the present work, a new analysis of the model is presented, showing that both the hard X-ray and microwave emissions originate in the same quasi-Maxwellian electron distribution; i.e., a natural consequence of the thermal model considered here is that the emissions have a common source. This is contrary to the results of previous analyses (BMS; Smith and

[1] Also Department of Physics and Astronomy, University of North Carolina, Chapel Hill. Present address: Space Department, The Johns Hopkins University Applied Physics Laboratory.

Brown 1980, hereafter SB), which are described in § II. In the context of a thermal-flare model, the common-source assumption provides a new observational test of the model: the rise time of the emission specifies a relation of size to temperature of the source, which can be compared with the relationship derived from the observed hard X-ray and microwave spectra. The source sizes are calculated by means of techniques first applied to the analysis of solar flares by Crannell *et al.* (1978). The calculation of the theoretical rise time is shown to be in excellent agreement with the new observations, as well as providing a physical basis for the analysis that was performed by Crannell *et al.*

In § II, the development of the model is described and arguments for a revised view of its predictions are set forth. In § III, the observations and the criteria used to select the flares are described, and the revised predictions are confronted with the observations. The conclusions are summarized in § IV.

II. THE THERMAL MODEL WITH CONDUCTION-FRONT CONFINEMENT

a) Development and Previous Applications of the Model

Conduction-front confinement of a thermal hard X-ray source was first studied in the solar-flare context by BMS. Spicer (1976, 1977*a*) had proposed magnetic reconnection via the tearing-mode instability as the energy-release mechanism for flares, and his calculations suggested that a preflare coronal arch would be most unstable to tearing-mode growth near its apex. Most of the energy released would go into heating the unstable portion of the arch (cf. Smith 1980). BMS therefore investigated the consequences of localized, impulsive heating of electrons at the apex of such an arch to a temperature $T_e \gtrsim 10^8$ K. (Current-driven instabilities such as the tearing mode chiefly heat the electron component of the plasma, rather than the bulk of the ions.) The result of this energy release is illustrated in Figure 1. The heated region was taken to be of length L at the time of maximum emission. $L \approx 10^4$ km was found to be consistent with observations. For reasonable coronal densities n_e of order 10^9–10^{11} cm^{-3} and electron temperatures characteristic of the hard X-ray spectra, the electron-ion energy equipartition time τ_{eq} is of order 10^4 s (Spitzer 1962); thus the ions would remain at their preflare temperature throughout the burst. In addition, under these conditions, the collisional mean free path of the hot electrons would exceed L. The hot electrons in such a region would begin to escape along the magnetic field lines, with negligible cross-field diffusion, and enter the gas in the lower parts of the arch, which would still be at preflare temperatures of $\sim 2 \times 10^6$ K. As shown by Spicer (1977*b*), the hot electrons, streaming into the cooler region, would induce a neutralizing reverse current of cooler electrons, with a drift velocity v_d which would exceed the ion-sound velocity, $c_s = (kT_e/m_i)^{1/2}$. For $v_d > c_s$, the plasma is unstable to the growth of turbulent ion-sound waves, which would grow in amplitude with an e-folding rate of the order of the ion plasma frequency, defined by the expression $\omega_i \equiv (4\pi n_i e^2/m_i)^{1/2}$. For the solar atmosphere, $m_i \approx m_p$, and the growth rate of the waves in a coronal arch with density $\sim 10^9$ cm^{-3} would be $\sim 10^7$ s^{-1}. The spectrum and directional distribution of the ion-sound waves is described by Horton and Choi (1979), both theoretically and as they are observed in comparable laboratory plasmas. Figure 2 illustrates these properties of the turbulent waves. The turbulent wave amplitude would grow for a few growth times—a few times 10^{-7} s—and would saturate

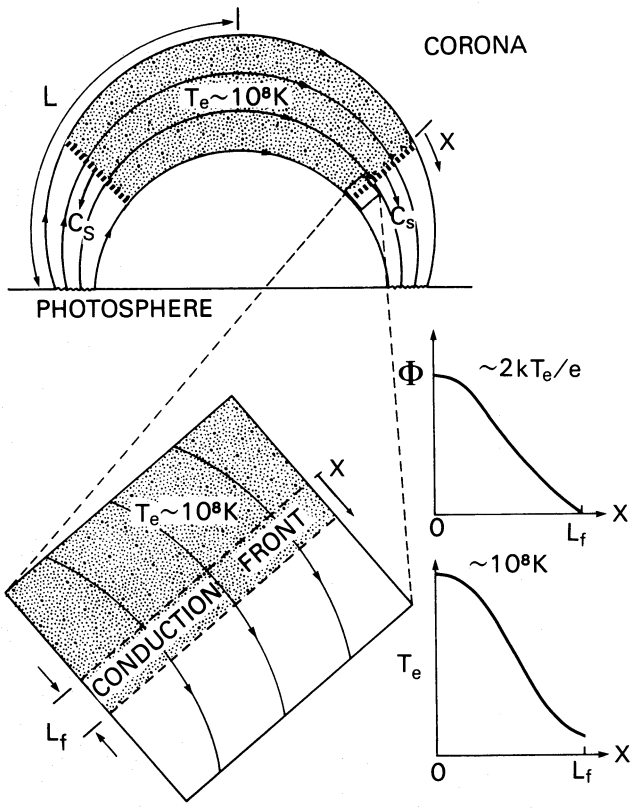

FIG. 1.—Schematic diagram of the thermal model with conduction-front confinement in a coronal arch. Shading indicates the confined, high-temperature electrons. A portion of the conduction front is expanded to indicate its thickness L_f. The front velocity is the ion-acoustic velocity c_s. The coordinate x is the distance along the arch in the direction away from its apex, as measured from the boundary of the front nearest to the apex. The graphs illustrate the variation of the electric potential due to the thermoelectric field and the temperature in the front.

with a total energy density in the waves $w_s \approx 10^{-2} w_T$, where w_T is the thermal energy density (pressure) in the plasma. The resulting ion-sound turbulence would be maintained at a marginally stable level in a relatively thin front at each end of the hot region, known as a collisionless conduction front. The conduction front would limit expansion of most of the hot electrons to the speed of propagation of the front, $\sim c_s$. Thus, the turbulence would serve as a confinement mechanism, insulating the hot electrons. Note also that, in the absence of the turbulence, the hot electrons would stream out of the source with a speed of order $v_e = (kT_e/m_e)^{1/2}$. For the solar atmosphere, with $m_i \approx m_p$, c_s is about $v_e/43$. Thus the turbulence would reduce the cooling rate of the source by about a factor of 43 below its free-streaming value. The turbulence also would effectively increase the collision rate of the electrons, leading to a relaxed electron distribution despite the low frequency of Coulomb collisions. The laboratory experience of Fowler (1968) suggests that the relaxed distribution would be nearly Maxwellian.

BMS and SL gave detailed derivations of the front thickness and showed that the front velocity is c_s. BMS identified the hard X-ray fall time of emission from such a source with the cooling time, $\tau_{cool} = L/c_s$.

SL proposed a similar physical picture but added several more realistic features. A one-dimensional, one-fluid, two-temperature numerical simulation was used to follow the evo-

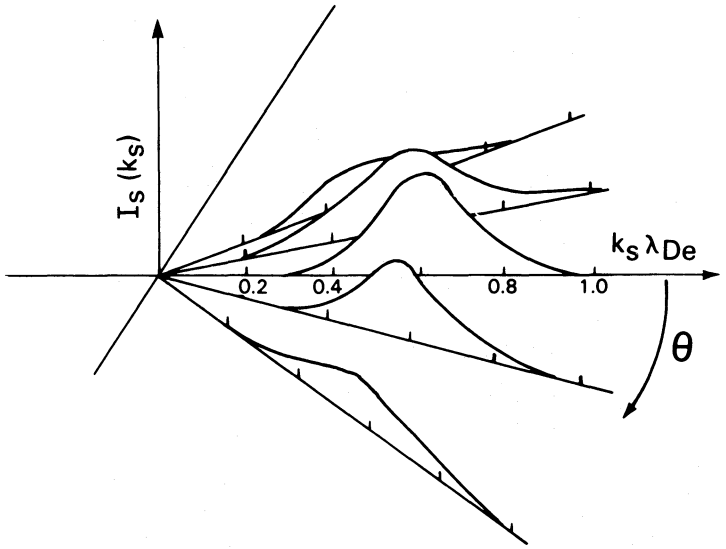

FIG. 2.—Distribution of amplitude of the ion-acoustic waves in the conduction front, as a function of the direction and magnitude of $\boldsymbol{k}_s$. The direction $\theta = 0$ corresponds to the negative x direction in Fig. 1. The quantity $I_s(k_s)$ is the amplitude of the ion-acoustic wave with wavenumber k_s. The wavenumber k_s is the radius from the I_s axis, expressed in the units $1/\lambda_{De}$. (Figure after Horton and Choi 1979.)

lution of a tube filled with plasma, continuously heated at its apex. This allowed the effects of convection to be taken into account. Continuous heating was also more realistic from an observational viewpoint; the temperature of hard X-ray bursts usually increases continuously until the time of maximum emission or later (e.g., Crannell *et al.* 1978; Wiehl *et al.* 1983). SL showed that conduction fronts indeed would develop in an arch 10^4 km in length with $n_e = 3 \times 10^{11}$ cm^{-3}. Computational problems limited the simulation to a duration of 0.74 s, however.

Smith and Auer (1980, hereafter SA) extended the duration of the simulation and studied the consequences of varying the heating rate and initial temperature, also using the same initial density as SL. They showed that, for the higher heating rates, the hot part of the arch divided into two regions of different temperatures, bounded by conduction fronts that advanced at velocities somewhat different from c_s. The two temperatures gave rise to a hard X-ray spectrum of the whole source that was indistinguishable from a power law over the photon energy range from 10 to 100 keV (cf. Brown 1974).

The most realistic simulation carried out to date, and the one with results of most relevance to the present work, was carried out by Smith and Harmony (1982, hereafter SH2). For the first time, the limit of the expansion of the source was studied. A model chromosphere was included at the feet of the arch. When the conduction front reached the chromosphere, the cooler, denser matter there mixed with the hot, tenuous gas of the hard X-ray source, quenching it. SH2 provided a time history of the resultant hard X-ray flux, summed over photon energies $\epsilon > 10$ keV, which resembles that of a simple, "spike" burst (compare Fig. 4 of SH2 with Fig. 1 of Crannell *et al.* 1978). The fall time of the emission was about equal to the rise time. (Similar results were obtained by Smith and Harmony 1981, hereafter SH1.) The result of SH1 and SH2 that is most important to the present analysis is that the peak of the hard X-ray time history occurred at the time when the conduction fronts reached the chromosphere and mixing began to quench the source.

Before discussing theoretical advances that pertain to the microwave emission, it is worthwhile to consider two objections that have been raised against the kind of model developed by BMS and Smith and collaborators, and to show that these objections can be refuted. First, there is the question of whether the model makes reasonable energetic demands. The energy source of solar flares is widely believed to be magnetic-field annihilation. Observations suggest that a component of magnetic field B of order 100 G is available for annihilation in active-region magnetic configurations. Annihilation of 100 G in a given volume yields only 400 ergs cm^{-3}. The numerical models of Smith and collaborators therefore have been criticized because they require much larger heating rates to be sustained for several seconds. For example, SA assumed heating rates in the range 1 to 8×10^4 ergs cm^{-3} s^{-1}. It should be noted, however, that these large heating rates were chosen to achieve the required temperatures for emission of hard X-rays ($\sim 2 \times 10^8$ K) specifically with an *assumed* density of 3×10^{11} cm^{-3}. If the density were two orders of magnitude smaller, e.g., a few times 10^9 cm^{-3}, the heating rate required to achieve the same temperature would be correspondingly smaller and thus consistent with a few hundred G of annihilated field. If the observations reported here are interpreted with the conduction front model, densities of a few times 10^9 cm^{-3} are indeed inferred, as shown in § III. Densities of this order are also consistent with those inferred from observations by Crannell *et al.* (1978) and agree with typical preflare densities observed in active regions.

As an aside, it may be noted that the densities of order 3×10^{11} cm^{-3} alluded to above would imply much smaller source volumes than are consistent with the microwave observations to be described herein.

A second objection to the model of BMS and SL was raised by Brown, Craig, and Karpen (1980, hereafter BCK). BCK argued that a single hot source, or kernel, of the kind examined by BMS, could not explain the observed spectral evolution. Their argument was based on the predicted relationship between the two parameters that specify the thermal brems-

strahlung spectrum: T_e and the emission measure, $\mu = n_e^2 V$, where V is the source volume. BCK assumed that a kernel was heated until the time of peak emission and that no further heating occurred thereafter. They also assumed that n_e remained constant. This assumption was considered justified because the expansion of the source is primarily a conductive process rather than a hydrodynamic expansion. Under these assumptions, if radiative energy losses can be neglected during the decline in emission from such a kernel, then conservation of energy implies that the quantity $\mu(t)T_e(t)$ would be constant, equal to $\mu_0 T_{e0}$, where the zeros designate values at the time of peak hard X-ray emission. T_e and μ, therefore, should be inversely related. The observed relationship had been studied by Mätzler *et al.* (1978), who presented correlation diagrams of T_e and μ for the flares of 1969 March 1 and 1970 March 1. In these two flares, the only events observed with sufficient counting statistics for such an investigation, T_e and μ were instead positively correlated. Having concluded that a single kernel of the BMS type could not explain these bursts, BCK then developed a more complex model in which numerous small kernels of the BMS kind were produced at a time-varying rate such that the observed relation between T_e and μ was the result.

The foregoing argument does not rule out the single-kernel model for two reasons. First, hydrodynamic motions play a role in the simulations of Smith and collaborators, a role which depends on the heating rate and can alter μ by changing n_e. BCK assumed n_e to be constant. Second, in the simulations of SH1 and SH2 the decline of hard X-ray emission is determined by competition between continuous heating and the convection or evaporation of cooler, chromospheric gas into the source, not just the conduction that BCK used to derive τ_{cool}. For both these reasons, the simple anticorrelation of T_e and μ resulting from the assumptions of BCK is not expected to hold in general. In fact, a variety of relationships between T_e and μ have been observed, some of them quite different from the correlations of Mätzler *et al.* (cf. Wiehl, Schöchlin, and Magun 1980; Wiehl *et al.* 1983). The relationship between T_e and μ in the simulations of SH1 and SH2 would clearly depend on the heating rate and its spatial variation, which the observations are still inadequate to determine. It appears likely that the model can reproduce the observed range of relationships by means of appropriate choices of the heating rate and its spatial variation, although this has not been investigated.

b) *The High-Energy Limit of Confinement and Its Implications for Microwave Emission*

For a Maxwellian distribution with $T_e \approx 10^8$ K in a region with $B \approx 100$ G, most of the microwave flux is emitted by electrons in the tail of the distribution with kinetic energy in the range $6kT_e \lesssim E \lesssim 12kT_e$ (Mätzler 1978). This corresponds to speeds of $v \approx 3v_e$ for typical sources considered in § III, for which $T_e \approx 3 \times 10^8$ K. It was first shown by BMS that the conduction fronts are transparent to tail electrons with velocities normal to the front in excess of some threshold. If the coordinate x is along the arch in the direction away from its apex, as shown in Figure 1, then the component of an electron's velocity normal to the front is v_x. A detailed calculation by SB suggested that this threshold was $v_x \approx 2v_e$, corresponding to a kinetic energy of $2kT_e$ associated with v_x (that is, $m_e v_x^2/2$). Thus the fraction of the distribution with $v < 2v_e$ ($E < 2kT_e$), approximately 74%, is confined by the conduction front.

As a result of the preceding analysis regarding escape of electrons with $E > 2kT_e$, no detailed predictions of microwave spectra were made by Smith and collaborators because they believed the microwave source electrons escape from the source, through the conduction fronts. Under these conditions, the escaping tail would not be relaxed, and would evolve independently of the thermal electrons. Consequently, the microwave emission has not been widely regarded as originating in a distribution of Maxwellian form, and the dynamics of the escaping tail have been treated as separate from the dynamics of the confined thermal electrons in this model. Flare emissions from electrons at energies above the threshold were studied qualitatively by Vlahos and Papadopoulos (1979). A particular functional form of the escaping electron distribution was considered by Emslie and Vlahos (1980), who calculated the resulting microwave spectrum and showed that it differed markedly from the spectrum of the confined source alone.

Clearly, then, the appropriateness of the treatment of the problem by SB, and the value of the escape threshold, are critical to any attempt to calculate the microwave spectrum expected in the conduction-front model. To begin, we shall reexamine the arguments advanced by SB regarding electron confinement and its consequences for microwave emission. In the following discussion, the analysis of SB is shown to be inadequate, primarily because the one-dimensional treatment of the electron velocities is inappropriate. Factors that contribute to a threshold effectively much higher than $2kT_e$ are then described. On the basis of these arguments, it is suggested that the confined source would in fact possess a well-developed Maxwellian tail, and that microwave emission with a spectrum characteristic of this distribution is expected, originating in the confined source.

i) *Limits on the Confinement of the Electrons Derived by SB*

The same one-dimensional expansion as studied by BMS and SL was considered by SB. In this latter work, however, the ion-acoustic waves excited in the conduction front were treated more realistically. BMS has assumed that the ion-acoustic turbulence was isotropic and that resonant scattering of the escaping electrons by the waves was the dominant confinement mechanism. Instead, theory and experiments with such current-driven waves show that only waves that propagate in directions within a cone of opening angle $\sim 45°$ around the direction of the return-current electron drift are excited (Sagdeev and Galeev 1969). As a result, the resonance condition that must be met for an electron to be scattered by the turbulent waves is $\omega_s \approx \boldsymbol{v} \cdot \boldsymbol{k}_s$, where ω_s is the frequency of the wave, $\boldsymbol{v}$ is the velocity of the electron, and $\boldsymbol{k}_s$ is the wave vector. For ion-acoustic waves, $\omega_s/k_s \approx c_s \ll v_e$. Because the waves propagate within 45° of the direction opposite the motion of the front, and because $v \approx v_e$ for the bulk of the electrons, the resonance condition can only be met for $\boldsymbol{v}$ approximately perpendicular to $\boldsymbol{k}_s$. In the one-dimensional analysis of SB, there are no electrons with such velocities. Hence, SB regarded resonant scattering of the hot source electrons by the waves as insignificant and concluded that scattering is not the dominant process that confines the hot electrons. Rather, in their analysis, the bulk of electrons are returned to the source by the thermoelectric field that develops within the front due to the electron temperature gradient $\partial T_e/\partial x$ (see Fig. 1). SB calculated the potential Φ due to the thermoelectric field, using marginal-stability conditions for the ion-acoustic turbulence, and showed that $\Phi \approx 2kT_e/e$. Consequently, only electrons with $v_x > 2v_e$ and kinetic energy $E > 2kT_e$ could surmount the

barrier and cross the front. Such electrons would thereby lose $2kT_e$ of kinetic energy in escaping from the confined thermal source. For these reasons, SB suggested that most of the microwave emission would come from the escaping component of the distribution, and they did not address the microwave emission any further. SB even questioned whether the escaping component could be produced by heating in a source confined by a collisionless conduction front. Citing the results of the numerical analysis by MacDonald, Rosenbluth, and Chuck (1957), SB argued that plasma heating would immediately establish an electron distribution with nearly Maxwellian form *only* for electron velocities $v \approx v_e$; the tail of the distribution, containing the microwave-emitting electrons, would require a few times $\tau_M(v') = \lambda(v')/v'$ to be populated up to velocity v'. The parameter $\lambda(v)$ is the electron collisional mean free path in the *absence* of turbulence (cf. Montgomery and Tidman 1964), given approximately by

$$\lambda(v) \approx 10^{-20} v^4/n_e \, . \tag{1}$$

For $v \approx 3v_e$, τ_M is typically a few seconds, about equal to the duration of the impulsive bursts to be explained. The time for such an electron to be lost by escape through the front is $\tau_s \approx L/v$. Characteristic source sizes are $L \approx 10^4$ km, so the streaming loss time $\tau_s \approx 0.01$ s. Because the loss time is much shorter than the production time of tail electrons by Coulomb collisions, few tail electrons would be expected to exist confined within the thermal source. Thus, the assumption that the effects of the turbulence on the distribution would be negligible led SB to conclude that the production of tail electrons in the confined source would be greatly inhibited and that the microwave emission from the confined source would be insignificant.

ii) *Population of the Maxwellian Tail and Resulting Microwave Emission*

An important question raised by SB was whether the Maxwellian tail could be populated rapidly enough to establish a relaxed Maxwellian distribution. Populating of the tail in a confined source would be enhanced by the resonant scattering of hot electrons in the front by the ion-acoustic waves. Resonant scattering increases the effective collision rate and causes the electron distribution to relax more rapidly than by means of Coulomb collisions alone. As noted above, the resonance condition is $\omega_s = \boldsymbol{v} \cdot \boldsymbol{k}_s$ ($\boldsymbol{v}$ approximately perpendicular to $\boldsymbol{k}_s$). SB regarded resonant scattering of the hot source electrons by the waves as insignificant because in their one-dimensional analysis, there are no electrons with such velocities. The analysis of SB leads to prediction of a truncated Maxwellian distribution in the confined source, poorly populated at $E \gtrsim kT_e$. If the analysis of SB were correct, it would then be necessary to postulate acceleration of nonthermal electrons, in order to explain the microwave emission, as done by Emslie and Vlahos (1980).

It appears, however, that the one-dimensional picture is misleading, and that the resonance condition can easily be met. For those electrons with $\alpha > 0$, a one-dimensional description of their trajectories is inadequate. (The pitch angle α is defined as $\tan^{-1}(v_+/v_x)$, where v_+ is the component of velocity perpendicular to $\boldsymbol{B}$). Consider a typical thermal electron in the confined source with $v_+ = v_x = v_e$. When this electron encounters the conduction front, the confining electric field reduces v_x continuously to $-v_e$; i.e., the electron is reflected by the potential barrier of the front. Near the turning point of its motion, $v_x \approx 0$, but $v_+ = v_e$. At this point, the resonance condition for scattering by the ion-acoustic waves is satisfied, and the electron is likely to be scattered into another part of the Maxwellian distribution. Actually, because the wave vectors $\boldsymbol{k}_s$ are distributed within a cone of about 45° half-opening angle, as shown in Figure 2, resonance can occur for pitch angles in the range $135° > \alpha > 45°$. The turbulent-wave intensity decreases with θ as shown in Figure 2, however, and a conservative estimate of the half-width of the wave spectrum is 22°. Thus electrons with $112° > \alpha > 68°$ are expected to interact with the waves. This resonant interaction relaxes the electron distribution by acting as a mechanism for energy exchange between the electrons, as shown next.

The effect of the turbulence on the electron-energy distribution function is found by consideration of the anomalous collision frequency, defined by the relation $\langle \boldsymbol{v} f_{\rm AN} \rangle \equiv \langle d\boldsymbol{v}/dt \rangle$. (The anomalous collision time $\tau_{\rm AN} = 1/f_{\rm AN}$ is the time required for wave-particle interactions to result in a change $\Delta \boldsymbol{v} \approx \boldsymbol{v}$ in an electron's velocity.) Because energy is conserved in a wave-electron collision, energy is transferred from electrons to waves to other electrons, leading to relaxation of those electrons in the distribution that interact with the waves. The turbulence increases the collision frequency from the Coulomb collision rate f_c to the anomalous collision frequency (SB; Sagdeev and Galeev 1969)

$$f_{\rm AN} \approx \frac{\omega_e u T_e}{4 v_e T_i} \left[\frac{e\phi}{kT_e} \right]^2 , \tag{2}$$

where u is the drift velocity of the current that maintains the turbulence, and $e\phi/kT_e$ is the ratio of energy in the waves to the thermal energy. In the present case, $u = c_s$. (Eq. [2] was derived for $u \gg c_s$, but the same result, within a factor near unity, was obtained by Mannheimer 1977, independent of this restriction.) It should be noted that $f_{\rm AN}$ is the actual exchange rate between electrons and ion-acoustic waves, not merely a rate for pitch-angle scattering of the electrons, as can be seen in Sagdeev and Galeev (1969), where an expression for it is derived from the quasi-linear equation for the electrons. SB derive $e\phi/kT_e$ self-consistently, finding the value

$$\left[\frac{e\phi}{kT_e} \right]^2 = \frac{8(2\pi)^{1/2}}{3\pi} \frac{k}{m_e \omega_e c_s} \frac{\partial T_e}{\partial x} \, . \tag{3}$$

Because the electrons are rapidly heated to $T_e \approx 10^8$ K while the ions remain at the preflare temperature $T_i \approx 10^6$ K, the ratio T_e/T_i can be set to ~ 100. The temperature gradient $\partial T_e/\partial x \approx T_e/L_f$, where L_f is the front thickness. The scattering mean free path of an electron in the turbulent region is $\lambda_{\rm AN} = v/f_{\rm AN}$, or, after substitution of the above values for $(e\phi/kT_e)^2$, T_e/T_i, and $\partial T_e/\partial x$,

$$\lambda_{\rm AN} \approx \frac{3\pi v}{200(2\pi)^{1/2} v_e} L_f \approx 0.02 \frac{v}{v_e} L_f \, . \tag{4}$$

Estimates of L_f vary from a fraction of 1 km (BMS) to 100 km (SA), but this expression shows that for $v \approx 3v_e$, $\lambda_{\rm AN} \ll L_f$, whatever value is chosen for L_f. Thus the turbulence will act to relax the distribution for values of v such that $\lambda_{\rm AN} \lesssim L_f$, subject to the condition that $112° > \alpha > 68°$ (for resonance to occur). In particular, the part of the high-energy tail in the electron distribution which is responsible for microwave emission, $v \approx 3v_e$, is populated by this relaxation process, as the following argument demonstrates.

Electrons with $v \lesssim 2v_e$ are confined in the thermal source by the electric field, and are part of the isotropic, Maxwellianized

bulk of the distribution. The number of microwave-emitting tail electrons trapped between the conduction fronts is determined by the rate equation

$$\dot{N}_{3,t} = r\dot{N}_{3,f} + \dot{N}_{3,h} - \frac{N_{3,t}}{\tau_{\rm loss}} . \quad (5)$$

In this equation, $N_{3,\ldots}$ denotes a number of electrons in the Maxwellian tail with $v \gtrsim 3v_e$, and in the resonant pitch angle range. The subscript t labels the total number of such trapped electrons. The subscript f labels the number of such electrons transferred from the bulk of the Maxwellian into the tail by interaction with the waves in the front. The subscript h labels the number of trapped tail electrons that are produced, if any, as a direct result of the heating process rather than wave interactions. Superposed dots indicate time derivatives. The variable r represents the fraction of tail electrons produced in the front that are confined in the trap. Because these electrons have high pitch angles, the thermoelectric field confines them, and we can assume r is approximately unity. For example, an electron with $v = 3v_e$ and $\alpha = 68°$ has a v_x of only $1.1v_e$, not enough to escape through the front. The variable $\tau_{\rm loss}$ represents the time scale for losses from the trap. This time scale is given roughly by $1/\tau_{\rm loss} = \sum_i 1/\tau_i$, where the terms τ_i represent time scales for the various loss processes.

The magnitudes of the terms in the rate equation can be estimated as follows. The first term, $\dot{N}_{3,f}$, is approximately equal to the number of electrons in the bulk of the distribution within the resonant pitch angle range multiplied by the energy exchange rate: $n_e V_f y(\alpha > \alpha_0) f_{\rm AN}$, where $V_f = \pi R^2 L_f$ is the volume of the front, R is the minor radius of the arch, and $y(\alpha > \alpha_0) \approx 0.39$ is the fraction of electrons in an isotropic distribution that lie in the resonant pitch-angle range. If we substitute the values $n_e \approx 10^9$ cm^{-3}, $T_e \approx 10^8$ K, derived from observations in § III, and $L_f \gtrsim 10^4$ cm, then $\dot{N}_{3,f} \gtrsim 10^{35}$ electrons s^{-1}. This is approximately the rate at which the tail is filled from the bulk of the distribution by resonant interactions. This rate can be taken as an extremely conservative lower bound, because the small front thickness of 100 km has been used.

The second term in the rate equation, $\dot{N}_{3,h}$, is an unknown function of the energy-release process. Information is not now available to specify it, but a nonzero value can only increase the tail population, so for a worst-case estimate we take it to be zero and consider the competing loss terms.

Tail electrons in the trap are subject to the following energy-loss processes: bremsstrahlung radiation, synchrotron radiation, source expansion, and escape due to Coulomb collisions. To calculate the loss time scales for these processes, we take a representative temperature of 3.5×10^8 K (30 keV) and consider a typical tail electron of velocity $3v_e = 2 \times 10^{10}$ cm s^{-1} with kinetic energy $E \approx 200$ keV. The bremsstrahlung and synchrotron losses are given by Ginzburg and Syrovatskii (1964). The bremsstrahlung-radiation loss time in the trap is approximately $\tau_b = 2 \times 10^{12} E[n_e(E/m_e c^2)]^{-1} = 10^6$ s. The synchrotron-radiation loss time in a magnetic field of 500 G is approximately $\tau_s = 10^6 E[B(E/m_e c^2)]^{-2} = 5 \times 10^3$ s. Expansion of the trap removes a fraction $4c_s/(3v_e \cos \alpha)$ of electron energy per traversal time of the trap, $L/(3v_e \cos \alpha)$. The trap length L is of order 10^9 cm, so the expansion loss time scale is $\tau_{\rm ex} = L/(4c_s) \approx 1$ s. Coulomb collisions scatter the electrons out of the source in a time of order $\lambda/v = 10^{-20} v^3/n_e \approx 10^2$ s. Thus the dominant loss mechanism is source expansion, and $\tau_{\rm loss} \approx 1$ s. At equilibrium, $N_{3,t} \approx 0.01 n_e V_{\rm trap}$. The loss term in the rate equation is roughly $N_{3,t}/\tau_{\rm loss} \approx 10^{32}$ electrons s^{-1}.

Comparing the production and loss rates derived in the preceding two paragraphs, we see that before the tail comes to equilibrium with the peak of the Maxwellian distribution, the tail is filled at a rate of order 10^{35} electrons s^{-1} and depleted at about 0.1% of this rate by loss processes. This shows that the resonant pitch-angle range will be essentially fully populated when equilibrium is reached between the bulk and tail of the distribution. This range, $112° > \alpha > 68°$, constitutes 39% of a full Maxwellian distribution, so 39% of the microwave-emitting tail electrons are expected to be present.

The effect of the absence of tail electrons with pitch angles $\alpha < 68°$ and $\alpha > 112°$ is negligible in the optically thick part of the microwave spectrum, which is of importance to the analysis in § III. An electron with pitch angle α emits a fraction $\sin^2 \alpha$ as much microwave radiation as one with a pitch angle of 90° and the same velocity. Thus the electrons in the range $112° > \alpha > 68°$ emit 27% as much radiation as an isotropic Maxwellian distribution of electrons. Because of the large optical depth in the sources to be considered, this reduction in emissivity does not affect source areas derived in § III.

Thus, the conduction-front model is consistent with the assumption of Crannell *et al.* (1978) that the temperature derived from observations of hard X-ray source electrons is also expected to characterize the microwave source electrons; indeed, for the pitch-angle range of the microwave source electrons, the same Maxwellian velocity distribution produces both hard X-rays and microwaves. This assumption is employed in the analysis of § III.

iii) *Reevaluation of the Confinement Limits*

Several factors ignored by SB contribute to better confinement of the tail electrons than is implied by the arguments in § II*b*(i). First, as demonstrated in the previous subsection, the one-dimensional analysis is misleading. Heating processes such as the tearing-mode instability are expected to lead to a nearly isotropic initial distribution of pitch angles. Electrons of total energy much greater than $2kT_e$ would be confined by the thermoelectric field, as long as the *component* of their velocity perpendicular to the conduction front, v_x, was less than $2v_e$. Because the magnetic field in the arch is also directed perpendicular to the conduction front, the confined electrons would have high pitch angles, and, consequently, emit microwaves with a high relative efficiency (cf. Ginzburg and Syrovatskii 1965).

A second factor contributing to enhanced confinement is that the thermoelectric field depends critically on the spectrum of the turbulent ion-acoustic waves. To simplify the calculation, SB in effect assumed a delta-function spectrum, peaked at wavenumber $k_s = 0.5/\lambda_{De}$ (where λ_{De} is the electron Debye length). The spectrum of waves in a real conduction front extends to higher wavenumbers (see Fig. 2, after Horton and Choi 1979). Contributions from higher wavenumbers would increase the thermoelectric field in a more realistic calculation. The value $\Phi = 2kT_e/e$ derived by SB is used in our discussion, but it should be considered a conservative lower limit. A higher value of Φ merely strengthens the arguments in this paper.

A third factor is the convergence of $\boldsymbol{B}$ observed in coronal arches near their feet in the chromosphere (cf. Spruit 1981). This convergence enables an arch to act as a magnetic bottle. The boundary of the loss cone is α_0, which is given by $\alpha_0 = \sin^{-1} (B_{\rm apex}/B_{\rm max})^{1/2}$. Electrons with pitch angles greater than

α_0 would be reflected from the region of converging field back into the source (cf. Boyd and Sanderson 1969). Most electrons that escaped through the conduction front, therefore, would be returned to the thermal source by magnetic reflection. The fraction of escaping electrons that return can be estimated as follows. For a conservative value of the mirror ratio, $B_{\rm apex}/B_{\rm max} = 0.5$, α_0 equals 45°. The fraction of escaping electrons that would be mirrored depends on their pitch-angle distribution. If the escaping electrons comprised an isotropic distribution, then approximately 70% of them would have pitch angles in the range $135° > \alpha > 45°$, and therefore would be reflected back into the source.

In fact, the pitch-angle distribution of the electrons escaping from the front is more favorable for reflection than that, as shown by the following considerations. In § II*b*(ii) it is shown that electrons with $E > 2kT_e$ can be produced with pitch angles in the range $135° > \alpha > 45°$, and, in fact, most will be produced in the range $112° > \alpha > 68°$. Those electrons that passed through the front would lose $2kT_e$ of kinetic energy in the x direction in surmounting the potential barrier of the front, resulting in the reduction of v_x relative to v_+. Thus all those that passed through the front would incur an automatic increase of pitch angle and be mirrored. (In returning to the thermal source, these electrons would regain the lost $2kT_e$, so there would be no net loss of energy by the tail electrons, and hence no net loss of electrons from the tail.) In a fully populated Maxwellian, electrons for which $E > 2kT_e$ make up approximately 26% of the distribution. According to the estimates in § II*b*(ii), the tail produced by resonant interactions with the anisotropic wave turbulence is at least 39% populated. Hence, the electrons in the tail comprise 10% of a fully populated Maxwellian. Electrons for which $E < 2kT_e$ make up approximately 74% of the distribution. Thus, the mechanisms postulated in this model will populate and confine 84% of a complete Maxwellian distribution.

To summarize the results of the foregoing discussion:

1. The rise time of the impulsive hard X-ray burst is expected to be L/c_s in the thermal model with conduction-front confinement and continuous heating.
2. The Maxwellian tail would be populated up to the energy range necessary for microwave emission by wave-particle interactions.
3. A three-dimensional treatment of the wave-particle interactions is necessary to properly characterize the electron distribution in the confined source, in contrast to the one-dimensional analysis of SB. When this is done, it is seen that more than 39% of the electrons with energies greater than the threshold calculated by SB would have pitch angles sufficiently high to be efficient producers of microwave emission and would be confined by the thermoelectric field or magnetic mirroring.

This picture is expected to be representative until the conduction fronts reach the chromosphere and are disrupted; the foregoing points constitute revised predictions of the model.

c) *Formulation of the Test Based on the Revised Predictions of the Model*

The model, incorporating the revisions discussed in § II*b*, can be tested using available observations. The observations have been analyzed under the following assumption: The electron distribution in the source can be approximated by a Maxwellian function with the temperature T_e resulting in the production of bremsstrahlung characterized by the best fit to the hard X-ray spectrum. This makes it possible to determine source parameters from the microwave and hard X-ray observations. The model leads to a prediction of burst rise times as a function of spectral parameters alone.

The conduction front is assumed to move at the ion-acoustic speed c_s. The solar atmosphere is mostly hydrogen, so m_i is m_p, the proton mass, and it follows that $c_s = 9100T_e^{1/2}$. The rise time t_r is equal to L/c_s, where L is the distance along the arch from the apex to the foot of the arch. Examination of the time histories shown by SH1 and SH2 indicates that the assumption of a constant front velocity equal to c_s gives t_r within a factor of 2. At the time of peak X-ray emission, L can be estimated from T_e and the microwave observations, as described by Crannell *et al.* (1978). The microwave spectrum usually rises with frequency f to a peak flux $S_{\rm max}$ at $f_{\rm max}$, and falls for $f > f_{\rm max}$. The part of the spectrum for which $f \lesssim f_{\rm max}$ is generally attributed to optically thick emission. For a homogeneous source, the spectrum is given by the Rayleigh-Jeans law:

$$S(f) = 1.36 \times 10^{-44} f^2 A_0 T_e , \qquad (6)$$

where S is the microwave flux density at Earth in solar flux units (1 sfu $= 10^{-22}$ W m^{-2} Hz^{-1}), f is the frequency in Hz, A_0 is the observed source area in cm^2, and T_e is the source temperature in K. To determine A_0, equation (6) is solved, using values of f and S in the optically thick part of the microwave spectrum obtained simultaneously with the measurement of T_e. The value of f to be used here is denoted f_2, the observing frequency below the observed $f_{\rm max}$. Use of f_2 ensures that the measurement is within the optically thick portion of the spectrum. The value $S_2 \equiv S(f_2)$ also is used. If the source is inhomogeneous and has an area that varies with f, $S(f)$ often exhibits a spectral index, $\alpha(f) = d \log S(f)/d \log f$, less than 2 (e.g., Mätzler 1978). In such a case, $S(f)$ is not given by equation (6), but the value calculated using that expression may be regarded as an effective area characterizing the source, and T_e must be similarly regarded as an effective temperature. Considerations of an appropriate model for such an inhomogeneous thermal source lead to the conclusion that the central, hottest part of the source is responsible for the optically thick emission of maximum frequency (Schöchlin and Magun 1979; Dulk and Dennis 1982). Because this hottest part also dominates the hard X-ray bremsstrahlung emission, the area calculated using f_2 and S_2 in equation (6) is, indeed, a physically significant value for A_0.

The time of peak X-ray flux is presumably the time when the conduction fronts reach the footpoints and the X-ray source just fills the entire arch. At that time, there is no room in the arch for a possible separate, escaped component of high-energy electrons which might complicate the microwave spectrum. Thus, S_2 and f_2 at the peak of the impulsive burst can be used to determine an A_0 characteristic of the entire arch.

The value of L must be derived from the observed area A_0, which is a function of three factors: the dimensions of the arch, the orientation of the arch, and the anisotropy of the microwave emission. The unknown dimensions of the arch are accounted for by the parameter $\eta \equiv 2L/w$, the ratio of total length of the arch to its average width. The value of η varies from arch to arch; a value of order 5 can be regarded as typical. A given arch, if viewed from the side, has a projected area of about $2Lw$. Rotation to another orientation can reduce this by as much as a factor of π. The effect of microwave anisotropy can reduce the observed area by another factor of order 2, as

can be seen by considering the simplified expression for f_{max} of Dulk and Marsh (1982):

$$f_{max} \approx 1.4(n_e w)^{0.1}(\sin\theta)^{0.6} T_e^{0.7} B^{0.9} . \quad (7)$$

In this expression, θ is the angle between the magnetic field direction and our line of sight, and B is in G. Because f_{max} is the frequency at which the emission changes from optically thick to optically thin, equation (7) also indirectly expresses the variation of optical depth with θ. Unless the arch is viewed directly from its side, θ varies from point to point along the arch, and consequently the section of the arch with the maximum value of θ dominates the spectrum at f_{max}. Sections with smaller values of θ are optically thick only at lower frequencies. Consideration of the weak dependence on θ in equation (7) suggests that this variation of optical depth with θ could reduce A_0 by as much as another factor of 2 in the case of a symmetrical arch. Because of the effects described in this paragraph, the inequality $A_0 \lesssim 2Lw \lesssim 2\pi A_0$ is expected to hold for each impulsive burst, resulting in an intrinsic scatter in the correlation between the observed rise times and those calculated with the present method.

It should be noted that the foregoing discussion of systematic uncertainties that contribute to the scatter may not be sufficiently exhaustive. For example, the arches could be nonuniform in temperature (cf. SA), and some arches could be asymmetrical, with different values of B at each foot. Each of these factors would affect the observed area. Imaging observations with good temporal and spatial resolution (which are not currently available) offer the only feasible means of sorting out these effects. On the other hand, if most flares occur in symmetrical arches with approximately uniform temperature, then the above inequality expresses the uncertainty in the predictions, as discussed below.

Substituting for w in the inequality and taking the square root yields

$$(\eta A_0)^{1/2}/2 \lesssim L \lesssim (\pi\eta A_0/2)^{1/2} . \quad (8)$$

It is useful to define the derived scale length,

$$L_0 \equiv A_0^{1/2} = 8.6 \times 10^{21}(S_2/T_e)^{1/2} f_2^{-1} . \quad (9)$$

The inequality becomes

$$\eta^{1/2} L_0/2 \lesssim L \lesssim (\pi\eta/2)^{1/2} L_0 . \quad (10a)$$

As an example, assuming typical arch dimensions, $\eta = 5$, leads to

$$1.1 L_0 \lesssim L \lesssim 2.8 L_0 . \quad (10b)$$

The measured rise time t_r should be within a factor of order unity of $\tau_0 \equiv L_0/c_s$, the derived time scale. More explicitly

$$\tau_0 = 9.4 \times 10^{17} S_2^{1/2}/(f_2 T_e) . \quad (11)$$

In general, the measured rise time is predicted to lie in the range

$$\eta^{1/2} L_0/2c_s \lesssim t_r \lesssim (\pi\eta/2)^{1/2} L_0/c_s . \quad (12a)$$

For a typical arch with $\eta = 5$,

$$1.1\tau_0 \lesssim t_r \lesssim 2.8\tau_0 . \quad (12b)$$

In summary, the model predicts a linear correlation between the measured rise time t_r and the parameter τ_0, computed from the spectral parameters. The constant of proportionality is predicted to be of order unity for typical arch dimensions. The best way to test this prediction is to construct a correlation plot of $\log t_r$ versus $\log \tau_0$, which is done in § III. An intrinsic scatter in the correlation is expected of about a factor of $2.8/1.1 = 2.5$ in the values of t_r.

It should be noted that Crannell *et al.* (1978) found a correlation of source area with event duration, derived from analysis of a set of simple impulsive spike bursts. They interpreted this correlation as evidence that burst dynamics are governed by the propagation velocity of a disturbance in the flare plasma, and suggested that the inferred velocities were comparable to either the ion-sound speed or the Alfvén velocity. They did not, however, investigate whether either of these possibilities was supported by their observations. The significance of their results for the model considered here is discussed further in § III*h*.

d) Other Derived Parameters

The average density also can be calculated from the projected area and emission measure μ. The volume of the arch is approximately $V = 2\pi L(w/2)^2$. From this formula, relation (10), and the definition of η, it follows that

$$\pi V_0/(4\eta^{1/2}) \lesssim V \lesssim \pi^{5/2} V_0/(2\eta)^{1/2} , \quad (13a)$$

where $V_0 \equiv L_0^3$ is the derived scale volume. For a typical arch with $\eta = 5$,

$$0.35 V_0 \lesssim V \lesssim 5.5 V_0 . \quad (13b)$$

From relation (13a) and the definition of emission measure, $\mu = n_e^2 V$, it follows that

$$\left[\frac{4\eta^{1/2}\mu}{\pi V_0}\right]^{1/2} \gtrsim n_e \gtrsim \left[\frac{(2\eta)^{1/2}\mu}{V_0}\right]^{1/2} \pi^{-5/2} , \quad (14a)$$

where $n_0 \equiv (\mu/V_0)^{1/2}$ is the derived scale density. For $\eta = 5$,

$$1.7 n_0 \gtrsim n_e \gtrsim 0.43 n_0 . \quad (14b)$$

(This estimate may be misleading, however, if there are large density gradients.)

The magnetic field in the plasma also can be calculated through the use of equation (7). Because the source is assumed to be an arch, the portions of the arch with maximum θ will dominate the emission. It is assumed here that $\theta = 80°$. The systematic uncertainty introduced by this assumption is small because of the weak dependence of f_{max} on $\sin\theta$. The very weak dependence of this expression on n_e and w allows mean values of these parameters to be used without introducing large uncertainties. If n_e is given the value n_0, and w is given the value $2L_0/5$, corresponding to $\eta = 5$, equation (7) can be solved for B, yielding

$$B = 0.77(n_0 L_0)^{-0.1} T_e^{-0.8} f_{max}^{1.1} . \quad (15)$$

Another quantity of interest is the thermal energy density in the plasma, $w_T = (3/2) n_e k T_e$ (assuming $T_e \gg T_i$, the ion temperature), easily obtained from relations (14a). The total energy of the thermal plasma is given by $U = w_T V$. The plasma β is defined as w_T/w_B, where $w_B = B^2/8\pi$ is the energy density associated with the magnetic field. (If the magnetic field is to be capable of preventing the source from expanding laterally, β must be less than unity. The dynamics of the emission would be so altered by the expansion anticipated in a high-β plasma that the analysis in this paper would be inadequate.) The quantities w_T, U, w_B, and β are uncertain by the same multiplicative factor as n_e, about 4 in the case of $\eta = 5$.

Useful estimates, w_{T0}, U_0, w_{B0}, and β_0, are derived by using n_0 as an estimate of n_e.

For the purpose of comparison with the prediction of the conduction-front model, the time for an Alfvén wave to cross the source is also of interest. If $v_A = B/(4\pi n_e m_p)^{1/2}$ is the Alfvén velocity, then $\tau_A \equiv L_0/v_A$ might be the characteristic time scale for energy release via a magnetic reconnection instability such as the tearing mode (cf. Brown and Smith 1980). Thus τ_A might be related to t_r, if the growth of a magnetic instability determined the growth of emission. The Alfvén time scale can be estimated as

$$\tau_A = 4.6 \times 10^{-12} B^{-1} L_0 n_0^{1/2} . \quad (16)$$

III. THE OBSERVATIONS AND THE TEST OF THE MODEL

a) *Instrumentation*

The hard X-ray observations were made with the Hard X-ray Burst Spectrometer (HXRBS) on board the *Solar Maximum Mission* spacecraft (*SMM*). The HXRBS uses an actively shielded CsI(Na) scintillation detector, and has been described in detail by Orwig, Frost, and Dennis (1980). Pulse height spectral data were obtained every 0.128 s for each of 15 channels distributed over the instrument's energy range of sensitivity. The energy range varied slowly and monotonically since launch. In 1980 March it was 26 to 456 keV, and in 1981 December it was 30 to 531 keV. A detailed description of this behavior and a listing of events observed with HXRBS are available in Dennis *et al.* (1983).

The microwave observations were made at Bern Observatory with 0.1 s time resolution. A description of the instruments at Bern has been given by Magun *et al.* (1981). For the flares analyzed herein, data are available at some or all of the following frequencies: 3.2, 5.2, 8.4, 10.4, 11.8, 19.6, and 35 GHz. Absolute flux densities were obtained by comparison with calibrated quiet-Sun measurements, as described by Wiehl *et al.* (1983). In two cases, time histories of 2.8 GHz emission obtained at Ottawa were used to supplement the coverage when no 3.2 GHz data were available.

b) *Event Selection*

Between 1980 February and 1981 December, 61 flares exceeding 500 sfu were observed at Bern. Of these flares, 26 also were observed with the HXRBS on *SMM*. For each of these flares, the plot of the hard X-ray counting rate summed over Channels 2 through 15 was examined for statistically significant impulsive increases by at least a factor of 2 in 30 s or less. Channel 1 was excluded because its width and calibration are not well known. The threshold of a factor of 2 was chosen because in some cases the impulsive rise was superposed on a clearly distinguishable gradual component, which was to be subtracted. In 23 of the events, such impulsive rises were found. These 23 bursts are listed in Table 1, with the locations on the solar disk of associated Hα emission. The impulsive rises analyzed in the present work occurred during the flares on this list.

Of the flares listed in Table 1, 13 have been investigated previously by Wiehl *et al.* (1983). Most of the impulsive rises considered here are different from the ones studied by Wiehl *et al.*, however, because of the different selection criteria.

c) *Selection of a Homogeneous Sample of Impulsive Rises*

During most of the flares, more than one impulsive rise occurred that satisfied the above criteria. To discriminate against superpositions of impulsive features that might originate in different locations on the Sun, only the first such rise in each flare was chosen. This set includes impulsive rises to a more-or-less constant "plateau" of emission as well as "spike" bursts that fell in roughly the same time as they rose. Such plateaus were not included in the similar analysis of Crannell *et al.* (1978). No systematic differences between the properties of the plateaus and those of the spikes are found in the results of this work.

To test the proposed model, two conditions must hold with respect to each impulsive rise in addition to the specified selection criteria. First, the optically thick portion of the microwave spectrum must be observed. Second, the entire source area must be observed. If part of the source were occulted by the solar limb, the derived value of L would be too low. Because Events 4, 11, and 23 were associated with Hα emission at the limb, and may therefore have occurred in partially occulted arches, they were excluded from the correlation analysis. The rises occurring in these limb events can be used as a consistency check, however, as is shown after the statistical analysis of a properly homogeneous set of events is complete. The remaining 20 rises were analyzed as a homogeneous sample. The three rises which were excluded from this group are noted in Table 1.

TABLE 1

TIMES AND POSITIONS OF IMPULSIVE RISES

Event Number	t_{peak} (UT)	Hα Position
1	1980 Mar 29 0918:10	N 27 E 38
2	1980 Mar 29 0955:07.1	N 07 W 10
3	1980 Jun 4 0654:19.6	S 14 E 59
4[a]	1980 Jun 29 1041:36	S 27 W 90
5	1980 Jul 1 1626:56.7	S 12 W 38
6	1980 Oct 9 1123:59.2	S 10 E 54
7	1980 Nov 6 0650:52	N 09 E 08
8	1980 Nov 8 1449:47	S 09 E 37
9	1980 Nov 8 1450:26	S 09 E 37
10	1980 Nov 8 1452:18.5	S 09 E 37
11[a]	1980 Nov 18 0718:09	S 10 W 90
12	1980 Dec 17 0845:37.7	N 10 E 03
13	1981 Mar 23 0655:51	N 10 W 54
14	1981 Apr 10 1644:53	N 09 W 37
15	1981 Apr 15 0643:09.6	N 20 W 65
16	1981 Apr 18 1049:28.5	unknown
17	1981 Apr 26 1115:32	N 12 W 74
18	1981 May 4 0838:03.8	N 16 E 19
19	1981 Jul 19 0533:31.5	S 29 W 56
20	1981 Jul 20 1311:33	S 26 W 56
21	1981 Jul 26 1350:00	S 15 E 27
22	1981 Aug 10 0658:50.9	S 13 W 15
23[a]	1981 Dec 7 1451:03	S 06 E 90

[a] Event not included in the statistical analysis because it occurred on the limb.

d) *Observed and Derived Parameters for Each Rise*

The hard X-ray time history, summed over Channels 2 through 15, was inspected to determine t_{peak}, the time of peak counting rate. Figure 3, including the time history for Event 7, serves as an example. In the cases of plateaus, t_{peak} was taken to be the time at which the counting rate stopped rising, excluding

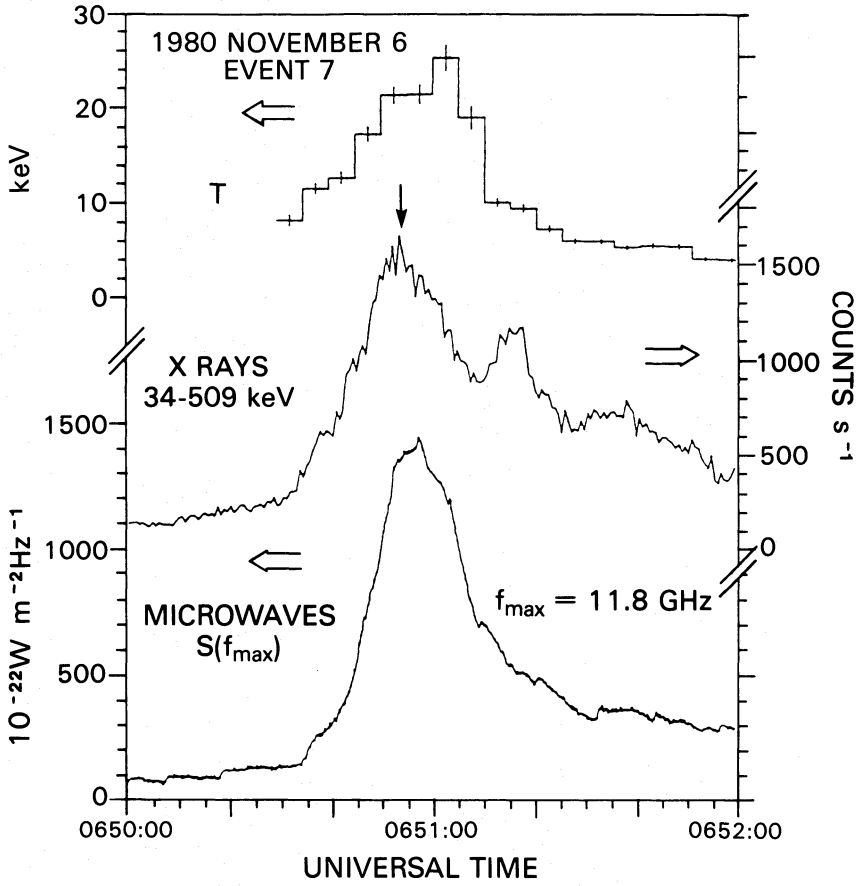

FIG. 3.—Time history of hard X-rays, microwaves, and best-fit temperature derived from dynamic hard X-ray spectra for impulsive rise number 7. The hard X-ray count rate is summed over channels 2 through 15. The microwaves are at the peak frequency. The derived hard X-ray temperature T is in the units keV. The vertical arrow indicates t_{peak}.

small fluctuations at a level consistent with stochastic fluctuations in the counting rate. An example of a plateau is shown in Figure 4. Three spikes such as the rise in Event 5, shown in Figure 5, exhibited significant structure near the peak. In such a case, if the counting rate dropped by as much as 10% and afterward resumed rising, t_{peak} was taken to be at the peak prior to the drop. From the standpoint of the model, this behavior could be interpreted as the result of heating at a point not precisely at the apex of the arch, as might occur in an asymmetrical arch (cf. Spicer 1976). It is also possible that these cases are examples of superposed impulsive features, despite efforts to exclude them. The values of t_{peak} are listed in Table 1.

The hard X-ray time history was inspected to measure the excess counting rate above background, I_{peak}, at t_{peak}. The time at which an excess count rate of $I_{peak}/2$ above background was attained, $t_{1/2}$, was determined as well. For cases in which the impulsive rise is superposed on a gradual component, as in Figure 5, the gradual flare emission was treated as background.

The quantity $t_r \equiv 2(t_{peak} - t_{1/2})$ was used as a measure of the observed rise time. Because small statistical fluctuations in the counting rate can introduce large uncertainties in the start time of the rise, t_r is a more precise measure of the rise time than $t_{peak} - t_{start}$. The values of t_r are listed in Table 2.

The microwave spectrum associated with each rise was constructed from observations at t_{peak}. Gradual microwave emission, analogous to the gradual hard X-ray emission, was similarly treated as background. The resulting spectrum was examined to determine S_2, f_2, and f_{max}. Two example spectra are presented in Figure 6.

For all the flares except Events 8, 10, 20, and 21, f_2 and S_2 could be determined from the Bern observations. In the case of Event 20, the optically thick part of the spectrum was not observed at Bern. In the absence of other data, this event would have been excluded. A time history at 2.8 GHz obtained at Ottawa was available, however, and this made it possible to determine S_2 at $f_2 = 2.8$ GHz. The spectrum of the rise in Event 8 was too flat for determination of the parameters. The spectrum of Event 10 had two peaks, and the optically thick portion of the peak at low frequency was not observed. The optically thick part of the spectrum of Event 21 was not observed at all. Consequently, calculations of the derived parameters could not be done for Events 8, 10, and 21, and they were not included in the statistical analysis.

Determinations of f_{max} could be made for most of the remaining 17 rises of the homogeneous sample. Only lower bounds on f_{max} could be found for Events 5, 11, 19, and 23, because f_{max} was greater than or equal to the highest frequency of observation, 35 GHz. In the case of Event 20, it was again necessary to use the Ottawa data at 2.8 GHz. The estimate $f_{max} \sim 5$ GHz was adopted.

Hard X-ray spectra were determined for each of the 20 rises from data accumulated for a time interval centered on t_{peak} of sufficient duration to obtain adequate counting statistics. An iterative technique, described in detail by Batchelor (1984), was

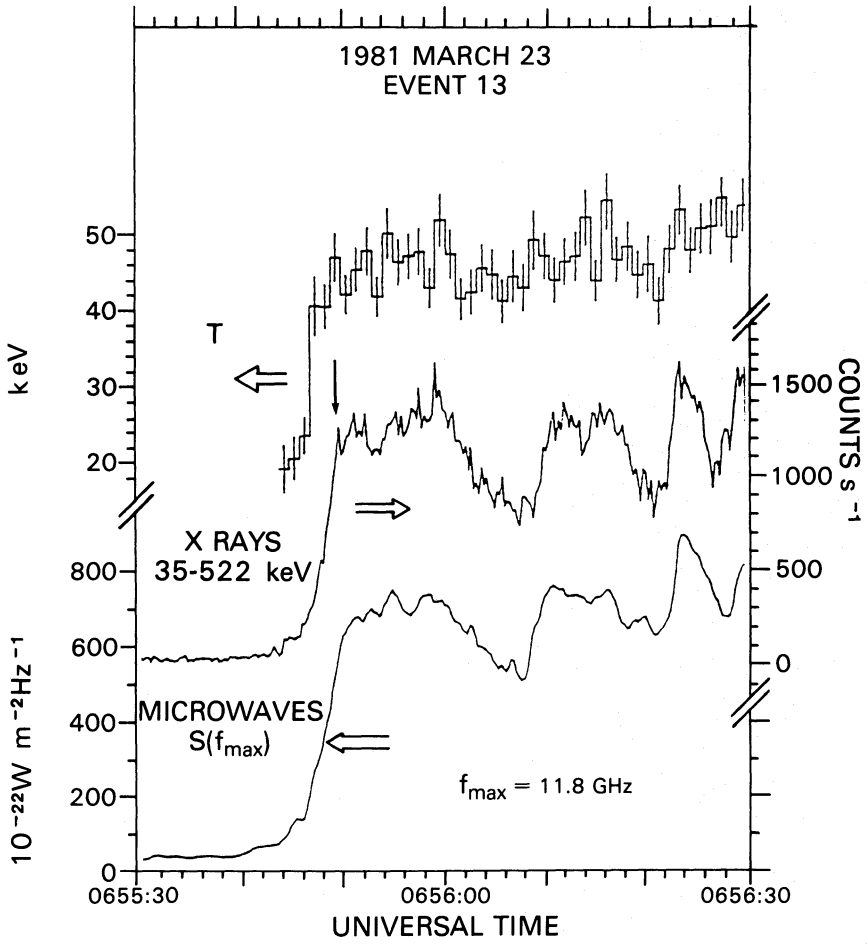

FIG. 4.—Same as Fig. 3, for impulsive rise number 13

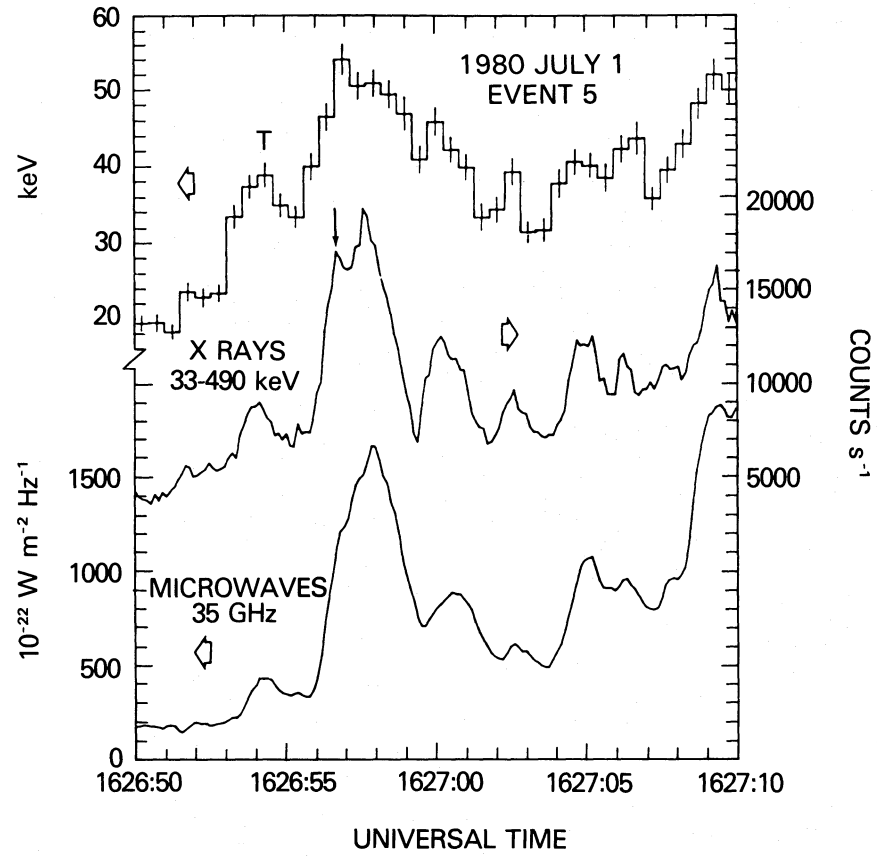

FIG. 5.—Same as Fig. 3, for impulsive rise number 5

TABLE 2

OBSERVED AND DERIVED PARAMETERS AT t_{peak}

Rise	S_2 (sfu)	f_2 (10^9 Hz)	f_{max} (10^9 Hz)	T_e (10^8 K)	μ (10^{45} cm^{-3})	t_r (s)	τ_0 (s)	L_0 (10^9 cm)	n_0 (10^9 cm^{-3})	w_{T0} (ergs cm^{-3})	U_0 (10^{27} ergs)	B (G)	w_B (ergs cm^{-3})	β_0	τ_A (s)
1.....	510	10.4	11.8	5.2	1.2	3.0	3.9	0.81	1.5	160	87	150	920	0.18	0.96
2.....	210	10.4	11.8	4.9	0.85	5.2	2.7	0.54	2.3	240	37	160	1000	0.23	0.74
3.....	320	8.4	11.8	3.9	8.5	7.0	5.1	0.91	3.3	280	210	170	1200	0.23	1.4
4[a].....	31	8.4	11.8	3.2	0.29	3.6	1.9	0.31	3.1	210	6.4	230	2100	0.10	0.34
5.....	460	19.6	$\gtrsim$35.0	6.4	1.0	0.9	1.6	0.37	4.5	600	30	$\gtrsim$420	$\gtrsim$6900	$\lesssim$0.087	$\lesssim$0.27
6.....	100	5.2	8.4	2.7	0.98	5.2	6.8	1.0	0.99	55	56	180	1300	0.041	0.80
7.....	910	8.4	11.8	2.4	0.56	20	14	2.0	0.27	14	100	300	3700	0.004	0.50
9.....	33	8.4	10	1.0	0.77	7.0	6.2	0.57	2.0	45	8.3	460	8500	0.005	0.25
11[a].....	44	19.6	$\gtrsim$35.0	2.9	0.16	2.2	1.1	0.17	5.7	350	1.7	$\gtrsim$820	$\gtrsim$27000	$\lesssim$0.013	$\lesssim$0.072
12.....	280	8.4	11.8	4.8	0.17	3.2	3.9	0.78	0.60	60	28	180	1300	0.046	0.49
13.....	260	8.4	11.8	4.9	0.33	6.0	3.7	0.74	0.90	92	37	170	1200	0.079	0.60
14.....	120	5.2	8.4	3.6	0.098	10	5.5	0.95	0.34	26	22	160	1000	0.025	0.50
15.....	14	5.2	8.4	1.9	0.27	3.8	3.6	0.45	1.7	67	6.1	250	2500	0.027	0.34
16.....	55	8.4	11.8	2.2	0.27	5.0	3.8	0.51	1.4	67	8.7	320	4100	0.016	0.27
17.....	75	3.2	5.2	2.7	0.50	11	9.5	1.4	0.42	24	66	110	510	0.046	1.2
18.....	17	5.2	10	2.2	0.68	1.8	3.4	0.45	2.7	120	12	250	2500	0.049	0.43
19.....	1400	19.6	$\gtrsim$35.0	3.5	3.3	12	5.2	0.87	2.2	160	110	$\gtrsim$660	$\gtrsim$18000	$\lesssim$0.009	$\lesssim$0.28
20.....	170	2.8	5	2.2	0.24	22	20	2.7	0.11	5	99	140	730	0.007	0.93
22.....	200	8.4	11.8	3.1	1.2	2.6	5.1	0.81	1.5	99	52	230	2100	0.047	0.62
23[a].....	240	19.6	$\gtrsim$35.0	5.8	0.74	10	1.3	0.28	5.8	710	15	$\gtrsim$450	$\gtrsim$8100	$\lesssim$0.088	$\lesssim$0.22

[a] Limb event. Derived parameters may not characterize whole source, if source is occulted.

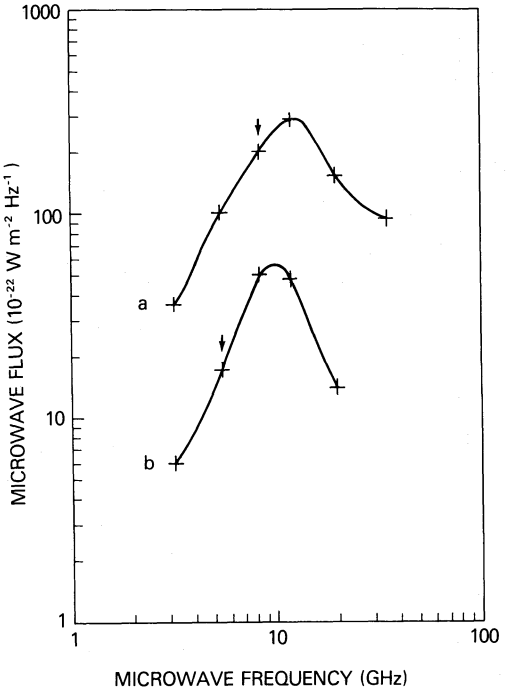

FIG. 6.—Microwave spectra at t_{peak} for Events 22(*a*) and 18(*b*). For each spectrum, f_2 is indicated by the vertical arrow.

used to determine the best linear least-squares fit between the data, corrected for instrumental effects, and the thermal bremsstrahlung function

$$I(E) = K_T E^{-1} T^{-1/2} G_E \exp\left[-(E - 50\ \text{keV})/T\right],$$

where K_T is a fitting parameter, E is the photon energy in keV, T is the best-fit temperature in keV ($T_e = 1.16 \times 10^7 T$), G_E is the total effective Gaunt factor, and $I(E)$ is the differential X-ray flux in photons $\text{cm}^{-2}\ \text{s}^{-1}\ \text{keV}^{-1}$. The thermal emission measure μ is

$$\mu = 9.3 \times 10^{41} K_T \exp(50\ \text{keV}/T)$$

in the units cm^{-3}. G_E was determined for $T_e < 5 \times 10^8$ K from Groenschild and Mewe (1978) and Mewe (private communication), assuming solar abundances giving an average value of $Z^2 = 1.355$. For $T_e > 5 \times 10^8$ K, G_E was calculated using the expressions given by Matteson (1971).

The derived parameters defined in §§ II*c*–II*d* could be calculated for the 20 events in which f_2 and S_2 were known; that is, for all rises except Events 8, 10, and 21. In Table 2, the observed parameters at t_{peak} and the derived parameters for the 20 rises are presented.

e) Correlation Analysis of Observed and Predicted Rise Times

The predictions of the model were tested as described in § II*c*. A linear correlation analysis was performed on the parameters t_r and τ_0 derived for each of the 17 impulsive rises that were not associated with Hα emission at the limb. The three limb rises were excluded, for reasons explained in § III*d*; they are considered separately in § III*g*(ii).

The relationship between t_r and τ_0 is presented graphically in Figure 7, and is $t_r = a(\tau_0)^b$, with some scatter. The parameters a and b are determined for the 17 disk events by means of an unweighted, linear least-squares fitting procedure. The values of a and b that are most representative of the relationship are found by minimizing the rms perpendicular distance of the 17 points from a straight line in the (log t_r, log τ_0) plane. This method was used to determine a and b. Two additional linear least-squares fits were carried out, one with respect to the t_r coordinate and one with respect to the τ_0 coordinate (Bevington 1969). The best fits derived by all three methods are indicated in Figure 7 with solid lines. The solid line with a slope intermediate between the other two represents the best fit derived by minimizing the rms perpendicular distance. The resulting parameters are: $a = 0.51$, $b = 1.5$, with a correlation coefficient $r = 0.84$; i.e., $t_r \approx 0.51\tau_0^{1.5}$. Calculations of the 1 σ uncertainties in a and b by propagation of errors lead to the ranges $0.28 < a < 1.1$ and $0.98 < b < 2.0$. Thus the correlation is indeed approximately a linear relationship, as predicted in § II*c*, and is consistent with equality, within the uncertainties. This agreement between the predicted time scale and the measured rise time provides strong support for the model.

The probability $P_c(r, N)$ that the (t_r, τ_0) parameter pairs come from an uncorrelated parent population is a quantitative measure of the statistical significance of the correlation, N being the number of points (Bevington 1969). For these 17 disk events, $P_c(r, N) = 2.4 \times 10^{-5}$; hence an accidental relationship with a correlation coefficient as large as 0.84 s is highly unlikely. One would have to analyze 710,000 bursts and construct 42,000 plots like Figure 7 to obtain a correlation this good by accident.

The observed scatter in the correlation is about a factor of 3, in good agreement with the factor of 2.5 estimated in § II*c*, considering the uncertainties noted. The area between the dashed lines represents the predicted range determined from the inequality (11) for arches with $2 < \eta < 4$, somewhat less than the typical value of 5. This range should not be regarded as precise, however, because of possible contributions from asymmetrical arches and temperature gradients, and because of uncertainties in the measurements, described in the following subsections.

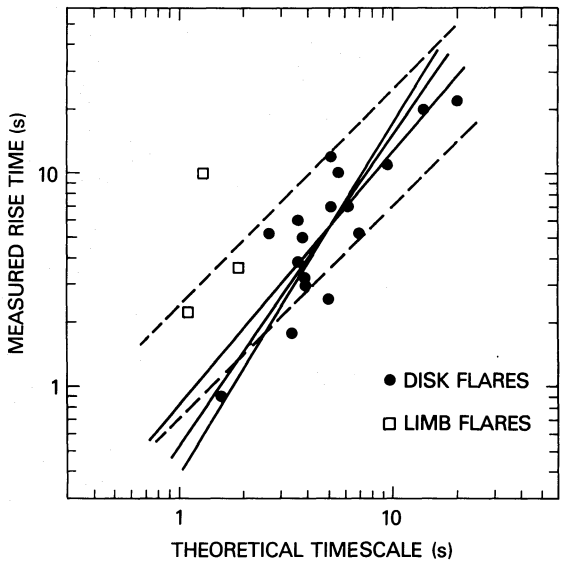

FIG. 7.—Correlation diagram of t_r and τ_0. Solid lines indicate best fits found by linear least-squares fitting. Dashed lines are boundaries of the expected positions of disk points, if the sources are arches from 2 to 4 times as long as they are thick.

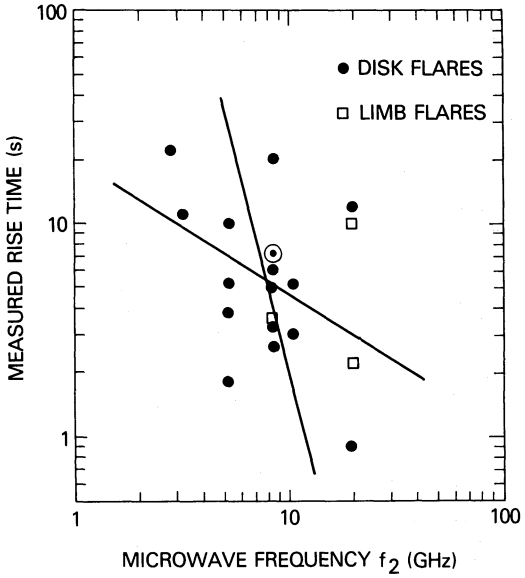

FIG. 8.—Plot of t_r vs. f_2. (Circled point indicates 2 overlapping points.)

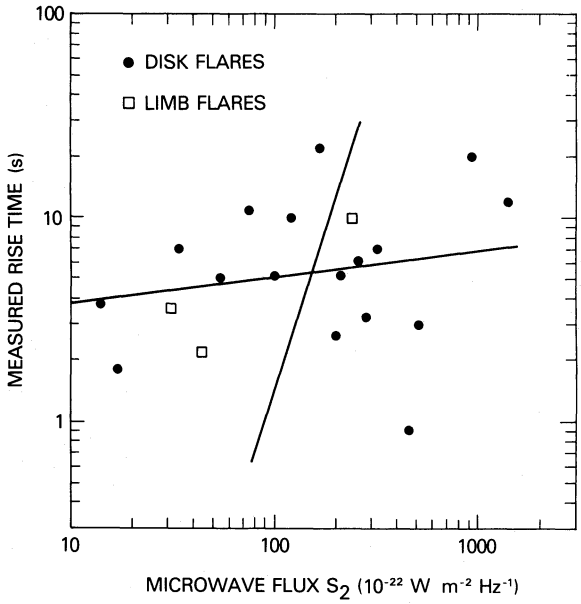

FIG. 9.—Plot of t_r vs. S_2

f) *Uncertainties in the Measurements*

Uncertainties in the measurements of f_2, S_2, and T_e contribute to uncertainty in τ_0. The choice of f_2 is not crucial to a precise calculation of τ_0, however. Only the value of $S^{1/2}/f$ in the optically thick part of the spectrum is required, with the qualification in the case of an inhomogeneous source that the frequency be as near f_{max} as possible (see § IIc). Determination of S_2 and f_2 as described in § IIc should not introduce uncertainties of more than 20% in the ratio $S^{1/2}/f$, including the uncertainties in S_2 alone. The uncertainty in T_e is also about 20%. Thermal fits were acceptable representations of the hard X-ray spectra from about 30 to 300 keV in most cases; in the remainder, the fit was acceptable at low energies but some excess was present at 100 keV or above. These excesses can be explained by departures from uniform temperature in the source, of the same magnitude as the uncertainty in T_e. The uncertainties in measurements of f_2, S_2, and T_e are therefore estimated to contribute much less to the scatter than the intrinsic uncertainties estimated in § IIc.

g) *Consistency Checks*

i) *Search for More Fundamental Correlations*

Consider first the possibility that the correlation between t_r and τ_0 is not the fundamental relationship revealed by Figure 7, but rather is the result of a relationship of t_r with some other parameter. The possible parameters are f_2, S_2, and T_e, and combinations of these parameters such as the derived length scale L_0 (c_s is proportional to $T_e^{1/2}$, so we need not consider it separately).

Correlation diagrams such as Figure 7 were constructed for the four possibilities, and are shown in Figures 8 through 11. The correlation diagrams for f_2, S_2, and T_e exhibit large amounts of scatter, and none has a correlation coefficient r greater than 0.40. Because this corresponds to a $P_c(r, N)$ of 0.1, it is clear that none of these parameters is the sole source of the relation of t_r and τ_0.

The relationship between L_0 and t_r was also considered. This possibility was suggested by a similar relationship found by Crannell *et al.* (1978) in a study of spike bursts (see § III*h*). In the case of L_0 and t_r, derived herein, L_0 is well correlated with t_r ($r = 0.81$, $P_c(r, N) = 8.1 \times 10^{-5}$). This result is to be expected because the values of c_s are all of the same order, in the range from 910 to 2300 km s^{-1}. The best-fit relationship is $L_0 \approx 0.30 \times 10^9 t_r^{0.57}$, and the correlation exhibits somewhat more scatter than that of t_r with τ_0. Thus, dividing L_0 by c_s produces a slightly better correlation, with $r = 0.84$, as opposed to $r = 0.81$ if L_0 alone is compared with t_r. The difference between these values of r is not a compelling argument in favor of the model but is consistent with the expectation that including the influence of c_s removes some of the variance in the observed relationship between t_r and L_0. Physical considerations, the existence of a model that predicts the observed

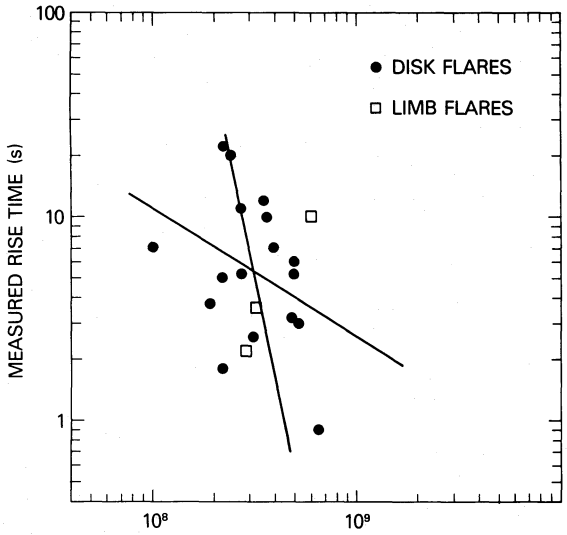

FIG. 10.—Plot of t_r vs. T_e

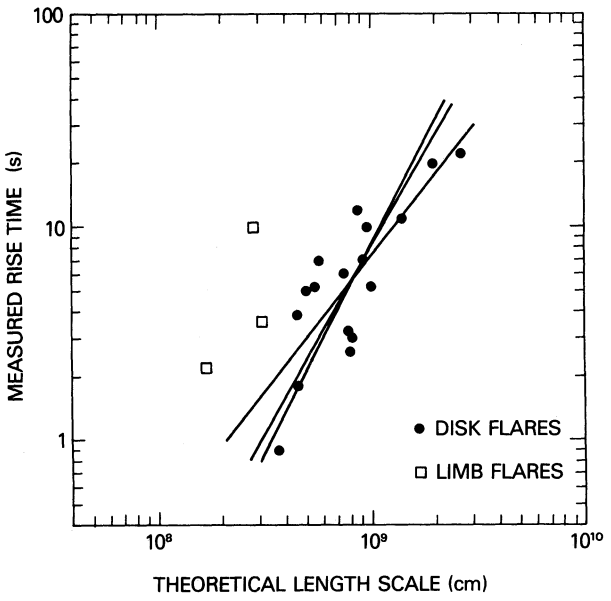

FIG. 11.—Plot of t_r vs. L_0

relationship between t_r and $\tau_0 \equiv L_0/c_s$, favor the interpretation inferred from the model.

ii) *Limb Rise Analysis*

Another check of the model is provided by the three limb rises that were observed. Partial occultation of the source by the solar limb in such cases might reduce the observed L_0, and therefore τ_0. Precise information about the source location with respect to the limb is not available. The area of a source precisely at the limb would not be occulted by a large fraction, and the corresponding point in Figure 7 would be near the least-squares fit of the disk sources. A source beyond the limb would be occulted, and the corresponding point would appear farther to the left of the least-squares fit in Figure 7.

Data on the three limb rises were reduced as described in § III*d*. The points corresponding to the limb rises in Figure 7 are all to the left of the best fit of the homogeneous group. The point for Event 23 appears farthest to the left ($t_r = 10$ s, $\tau_0 = 2.8$ s), suggesting that occultation by the solar limb reduced its apparent area by a large fraction, approximately 90%. All three of these cases are consistent with the prediction of the model and provide additional support for it.

It is also noteworthy that the values of L_0 derived for the limb rises are the three lowest values in Table 2. This is also consistent with the interpretation that they are partially occulted. It is remarkable that this interpretation can be made from observations with no spatial resolution.

h) Comparison with Results of Crannell et al. (1978)

The correlation of L_0 and t_r presented here can be compared to a similar result of the spike-burst study by Crannell *et al.* (1978). A correlation was found in that study between D, the derived source diameter in units of 10^9 cm at the time of peak microwave emission, and t_x, the burst duration in hard X-rays (the rise time plus the fall time). Because the rise and fall times of the spike bursts are approximately equal, t_x is approximately twice the rise time, t_{xr}. The best-fit relationship $t_x \approx 3.8D^{0.68}$ was found ($r = 0.80$, $P_c = 2 \times 10^{-4}$). To investigate whether this is consistent with the prediction of the model, the parameters S_2, f_2, T, and the actual t_{xr} measured by Crannell *et al.* for 16 of the spike bursts were used to calculate the corresponding L_0 and t_r. For comparison, the length scales D and L_0 for both sets of measurements are reexpressed in units of 10^9 cm and designated L_9. The rise time used herein is $t_r \approx 4t_{xr}/3$. The spike bursts exhibit the relationship $t_r = aL_9^b \approx 13L_9^{0.57}$. The 1 σ uncertainties in fitting parameters give $9.7 < a < 25$ and $0.40 < b < 1.0$. For comparison, the relationship shown in § III*g*(i) is $t_r \approx 8.3L_9^{1.7}$. The 1 σ uncertainties in this relationship are $6.3 < a < 12$ and $1.0 < b < 2.4$. Both of these relationships are consistent to within 1 σ with the prediction of the model, $b \approx 1$, with $a \approx 10$. This value of a corresponds to a mean ion-sound velocity of ~ 1000 km s^{-1} and electron temperature of $\sim 10^8$ K for the disk events. A correlation similar to that shown in Figure 7 was also present in the spike-burst study: $t_r \approx 5.4\tau_0^{0.49}$, with a correlation coefficient $r = 0.75$. The 1 σ uncertainties in this relationship are $2.3 < a < 6.8$ and $0.33 < b < 1.0$. Thus, this result too is consistent with a linear relationship between t_r and τ_0, as predicted by the model.

Crannell *et al.* interpreted the correlation of burst duration with derived diameter as support for the possibility that a compressional disturbance could traverse the source region and cause the required heating on time scales consistent with the time structures of the observed emissions (as in their adiabatic compression model). Velocities in the range from 200 to 700 km s^{-1} were inferred from the relationship between diameter and duration and attributed to such compressional disturbances. This result, however, was never related to a specific travel time of the disturbance.

Observational bias is present in both the spike-burst study and the present work. The flares listed in Table 1 were selected because of their large peak microwave fluxes and include relatively more large bursts than the sample of spike bursts, which were selected on the basis of the X-ray time histories. Thus the results presented here may be biased in favor of the properties of large bursts. As shown by Figure 9, there is no significant correlation of S_2 with t_r, however, and the average value of L_0 in the present study differs from that of the spike-burst events by only about 10%. Thus the excess of large bursts in the present study does not appear to contribute to systematic differences from the spike-burst results. A factor that may contribute to a systematic difference in the exponents of τ_0 is the lower sampling rate of the *OSO-5* X-ray data which were used in the spike burst study. Spectral data were measured by the spectrometer on *OSO-5* for a 0.19 s interval, every 1.9 s; HXRBS accumulates spectral data for each 0.128 s, continuously. Undersampling of the *OSO-5* data would introduce a systematic overestimate of t_r for X-ray variations on time scales of the order of the sampling interval or less, or disguise some multiply impulsive events as single spikes. Both these effects would contribute to the relatively low exponent of τ_0 derived from the *OSO-5* measurements. Future verifications of these correlations should make use of data with the best possible time resolution and a sample of bursts that is unbiased with respect to intensity.

In summary, the results of this work and the spike-burst analysis of Crannell *et al.* together provide strong support for the model.

i) Other Derived Parameters

The derived lengths, densities, and values of β are all consistent with the assumptions of the model. The length scales of the

rises observed on the solar disk vary from 3700 km to 27,000 km, which is a representative range of lengths for coronal arches. The densities are appropriate to arches in the corona, ranging from 0.11 to 4.5 × 10^9 cm^{-3}. The values of β are less than unity, showing that the neglect of lateral expansion in the heated arch is justified. The low β's also indicate that the energy requirements are not too great to be supplied by annihilation of a fraction of the derived magnetic field within the volume. The total energy inferred in the plasma, U_0, ranges from $\sim 10^{27}$ to $\sim 10^{29}$ ergs. This is quite modest in comparison with the requirements of nonthermal models, which range from $\sim 10^{28}$ to $\sim 10^{32}$ ergs (Brown and Melrose 1977).

As mentioned in § II*d*, the burst rise time t_r might also be related to the time required for an Alfvén wave to cross the source, τ_A. Figure 12 is the correlation diagram of t_r and τ_A. No significant correlation of the parameters is found [$P_c(r, N) = 0.28$]. Thus, no evidence is found for the hypothesis that the rise time of a burst is determined by the time for an Alfvén wave to traverse the source.

IV. CONCLUSIONS AND SUGGESTIONS FOR FUTURE INVESTIGATIONS

In this paper, new observational support is presented for the thermal-flare model which was proposed by Brown, Melrose, and Spicer (1979) and Smith and Lilliequist (1979). The observed relationship between the burst dynamics and the parameters of the microwave and hard X-ray spectra has not been predicted by any other model presented in the literature. The high degree of statistical significance of the correlation presented in § III*e* is clearly indicative of some fundamental underlying physical process that demands to be explained, whatever model is chosen for these impulsive bursts.

These results are particularly difficult to explain in the context of either of the major competing nonthermal models, the thick-target model or the trap-plus-precipitation model. In the thermal-conduction-front model, the calculation of predicted rise time τ_0 from spectral parameters depends on the thermal interpretation of the hard X-ray and microwave spectra and the characteristic expansion rate of a confined, thermal source. For either nonthermal model to be successful, it also would be required to explain the specific relationships between observed rise time and spectral parameters of the hard X-ray and microwave emissions. In the thick-target model, however, the rise time of a burst is determined by the dynamics of an unknown acceleration mechanism. The travel time of freely streaming nonthermal electrons from the apex to the footpoint of an arch in the thick-target model is of order 0.1 s, too short to be of relevance for the rise time of a burst. The thick-target model has not been shown to imply a specific relationship between rise time, source size, and nonthermal electron distribution, such as is necessary to explain Figure 7. In the trap-plus-precipitation model, the acceleration time scale, the escape time scale of the precipitating component of the electron distribution, and the effects of trapping or reacceleration would all have to compete in just such a way as to yield a rise time consistent with Figure 7. Neither of these models have been found to present any *a priori* physical reasons for the observed correlations.

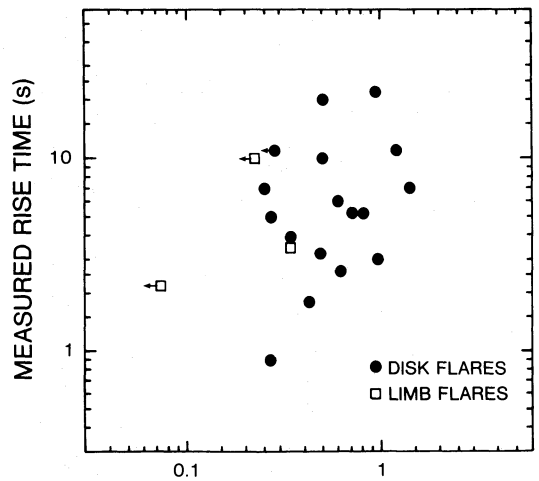

FIG. 12.—Plot of t_r vs. τ_A, the time for an Alfvén wave to cross the source

In the thermal-conduction-front model, the confinement mechanism leads in a straightforward way to the observed relationship of the parameters. That some correlation exists between the observed and derived rise times is, perhaps, not surprising, but the fact that the correlation is consistent with equality strongly suggests that the model has physical significance. These results also suggest that the model proposed by Brown, Craig, and Karpen (1980), which invokes many separate thermal sources with very short lifetimes, is not required to explain the observations.

Another interesting aspect of the conduction-front model that has not been investigated is the implication of the existence of the thermoelectric field in the conduction front for proton and ion acceleration. While this field has the effect of confining electrons within the thermal source, its direction is such as to accelerate positively charged particles out of the source. The potential, $\Phi = 2kT_e/e$, could accelerate protons to energies of order 50 keV, and ions of charge Z could reach proportionally higher energies. The possibility that the thermoelectric potential is actually higher than the value derived by Smith and Brown (1980) is also relevant to ion acceleration.

The results of this work are amenable to further testing by means of statistical analysis of additional rises and by means of imaging observations. The method used here to derive source sizes has never been tested by direct comparison with interferometric microwave observations or hard X-ray images. Additional theoretical development of the model would also be useful, in the form of improved fluid MHD simulations and particle simulations. These simulations could illuminate the detailed physics of the decline in emission, which is not considered here, and, perhaps, provide detailed explanations of the observed relationships between temperature and emission measure.

An instrument for imaging of hard X-rays in the energy range from 2 to 120 keV is being considered as part of the Pinhole/Occulter Facility, which has been proposed for use with Spacelab on a future Space Shuttle mission (Tandberg-Hanssen *et al.* 1983). With its proposed angular resolution of less than 1″ and subsecond time resolution, this instrument could provide an important test of the predictions of the model considered herein. Concurrent observations with such an instrument and a microwave interferometer with similar temporal and spatial resolution would be ideal for testing theoretical models of the flare phenomenon.

We wish to thank B. R. Dennis, L. E. Orwig, and K. J. Frost of NASA/GSFC for access to the Hard X-Ray Burst Spectrom-

eter data and analysis facilities, and for kind advice and assistance that contributed much to this work. The data reduction was greatly facilitated by the use of the excellent HXRBS data-analysis software, for which T. Chewning, H. E. Dennis, A. K. Tolbert, and J. Bonomo were responsible. G. S. Kennard and B. E. Gibson assisted in the use of that software. We wish to thank J. Gurman and D. Pothier for help in the use of the VAX 11/750 at the *SMM* Experimental Operations Facility. E. Sullivan and C. Hughes provided additional programming and data-processing assistance with the PDP 1144 in the Laboratory for Astronomy and Solar Physics.

Helpful discussions of this work with W. A. Christiansen, J. C. Brown, D. J. Forrest, A. L. Kiplinger, D. F. Smith, D. S. Spicer, and L. Vlahos are gratefully acknowledged. The comments of an anonymous referee also led to significant improvements in the paper.

This research was performed by D. A. B. at NASA/GSFC in partial fulfillment of the degree of Doctor of Philosophy in Physics from the University of North Carolina, Chapel Hill. The members of the dissertation committee were W. A. Christiansen, C. J. Crannell, B. W. Carney, W. J. Thompson, and J. W. York, Jr. D. A. B. was supported in part under contract NAS 5-26341 through Energy/Environmental Research Group of Tucson, Arizona. Additional support was provided under grant NSG 5066 through the Catholic University of America. Funding for both the contract and the grant was provided via the Goddard Space Flight Center from the Solar and Heliospheric Physics Office and the Solar-Terrestrial Theory Program of NASA Headquarters. For the past year, D. A. B. was supported as a NASA Graduate Student Researcher at the Laboratory for Astronomy and Solar Physics at Goddard Space Flight Center.

REFERENCES

Batchelor, D. A. 1984, Ph.D. Dissertation, University of North Carolina at Chapel Hill, published as *NASA Technical Memor.* No. 86102.
Bevington, P. R. 1969, *Data Reduction and Error Analysis for the Physical Sciences* (New York: Barnes and Noble).
Boyd, T. J. M., and Sanderson, J. J. 1969, *Plasma Dynamics* (New York: Barnes and Noble).
Brown, J. C. 1974, in *IAU Symposium 57, Coronal Disturbances*, ed. G. Newkirk (Dordrecht: Reidel), p. 395.
———. 1975, in *IAU Symposium 68, Solar Gamma, X-, and EUV Radiation*, ed. S. R. Kane (Dordrecht: Reidel), p. 245.
———. 1976, *Phil. Trans. Roy. Soc. London*, **281**, 473.
Brown, J. C., Carlaw, V. A., Cromwell, D., and Kane, S. R. 1983, *Solar Phys.*, **88**, 281.
Brown, J. C., Craig, I. J. D., and Karpen, J. T. 1980, *Solar Phys.*, **67**, 143 (BCK).
Brown, J. C., and Melrose, D. B. 1977, *Solar Phys.*, **52**, 117.
Brown, J. C., Melrose, D. B., and Spicer, D. S. 1979, *Ap. J.*, **228**, 592 (BMS).
Brown, J. C., and Smith, D. F. 1980, *Rept. Progr. Phys.*, **43**, 125.
Chubb, T. A. 1972, in *Solar-Terrestrial Physics/1970: Part I*, ed. E. R. Dyer (Dordrecht: Reidel), p. 99.
Colgate, S. A. 1978, *Ap. J.*, **221**, 1068.
Crannell, C. J., Frost, K. J., Mätzler, C., Ohki, K., and Saba, J. L. 1978, *Ap. J.*, **223**, 620.
Dennis, B. R., Frost, K. J., Orwig, L. E., Kiplinger, A., Dennis, H. E., Gibson, B. E., Kennard, G. S., and Tolbert, A. K. 1983, *NASA Technical Memo.*, No. 84998.
Dulk, G., and Dennis, B. 1982, *Ap. J.*, **260**, 875.
Dulk, G. A., and Marsh, K. A. 1982, *Ap. J.*, **259**, 350.
Emslie, A. G., and Vlahos, L. 1980, *Ap. J.*, **242**, 359.
Fowler, T. K. 1968, in *Advances in Plasma Physics*, Vol. **1**, ed. A. Simon and W. B. Thomson (New York: Interscience), p. 201.
Ginzburg, V. L., and Syrovatskii, S. I. 1964, *The Origin of Cosmic Rays* (New York: Macmillan).
———. 1965, *Ann. Rev. Astr. Ap.*, **3**, 297.
Groenschild, E. H. B. M., and Mewe, R. 1978, *Astr. Ap. Suppl.*, **32**, 283.
Horton, W., and Choi, D. 1979, *Phys. Rept.*, **49**, 273.
Hoyng, P., Brown, J. C., and van Beek, H. F. 1976, *Solar Phys.*, **48**, 197.
Hoyng, P., Knight, J. W., and Spicer, D. S. 1978, *Solar Phys.*, **58**, 139.
MacDonald, W. M., Rosenbluth, M. N., and Chuck, W. 1957, *Phys. Rev.*, **107**, 350.
Magun, A., Fuhrer, M., Kaempfer, N., Staehli, M., Schöchlin, W., Wiehl, H. 1981, *Inst. Appl. Phys. Rept.*, No. 46, University of Bern, Switzerland.
Mannheimer, W. M. 1977, *Phys. Fluids*, **20**, 265.
Matteson, J. L. 1971, Ph.D. thesis, University of California, San Diego.
Mätzler, C. 1978, *Astr. Ap.*, **70**, 181.
Mätzler, C., Bai, T., Crannell, C. J., and Frost, K. J. 1978, *Ap. J.*, **223**, 1058.
Melrose, D. B., and Brown, J. C. 1976, *M.N.R.A.S.*, **176**, 15.
Montgomery, D. C., and Tidman, D. A. 1964, *Plasma Kinetic Theory* (New York: McGraw-Hill), p. 30.
Orwig, L. E., Frost, K. J., and Dennis, B. R. 1980, *Solar Phys.*, **65**, 25.
Sagdeev, R. Z., and Galeev, A. A. 1969, *Nonlinear Plasma Theory* (New York: Benjamin), § III-2, pp. 94–103.
Schöchlin, W., and Magun, A. 1979, *Solar Phys.*, **64**, 349.
Smith, D. F. 1975, *Ap. J.*, **201**, 521.
———. 1980, *Solar Phys.*, **66**, 135.
Smith, D. F., and Auer, L. H. 1980, *Ap. J.*, **238**, 1126 (SA).
Smith, D. F., and Brown, J. C. 1980, *Ap. J.*, **242**, 799 (SB).
Smith, D. F., and Harmony, D. W. 1981, in *Plasma Astrophysics* (ESA SP-161), p. 401 (SH1).
———. 1982, *Ap. J.*, **252**, 800 (SH2).
Smith, D. F., and Lilliequist, C. G. 1979, *Ap. J.*, **232**, 582 (SL).
Spicer, D. S. 1976, *NRL Rept.*, No. 8036.
———. 1977*a*, *Solar Phys.*, **53**, 305.
———. 1977*b*, *Solar Phys.*, **54**, 379.
Spitzer, L., Jr. 1962, *Physics of Fully-Ionized Gases* (New York: Wiley-Interscience).
Spruit, H. C. 1981, in *The Sun as a Star*, ed. S. Jordan (NASA SP-450), p. 385.
Tandberg-Hanssen, E. A., Hudson, H. S., Dabbs, J. R., and Baity, W. A. 1983, *NASA Technical Paper*, No. 2168.
Vlahos, L., and Papadopoulos, K. 1979, *Ap. J.*, **233**, 717.
Wiehl, H. J., Batchelor, D. A., Crannell, C. J., Dennis, B. R., and Price, P. N. 1983, *NASA Technical Memo.*, No. 85052; also (condensed form) *Solar Phys.*, in press.
Wiehl, H. J., Schöchlin, W. A., and Magun, A. 1980, *Astr. Ap.*, **92**, 260.

D. A. BATCHELOR: Applied Physics Laboratory, Johns Hopkins Road, Laurel, MD 20707

C. J. CRANNELL: Code 682, NASA/Goddard Space Flight Center, Greenbelt, MD 20771

A. MAGUN and H. J. WIEHL: Institute for Applied Physics, University of Bern, CH-3012 Bern, Switzerland